IEEE Access
Multidisciplinary | Rapid Review | Open Access Journal

Date of publication xxxx 00, 0000, date of current version xxxx 00, 0000.

Digital Object Identifier 10.1109/ACCESS.2024.0429000

Digital Twin-Based Real-Time Blockage Detection for Liquid-Cooled Power Electronic Systems

Josiah N. Worch[1], Kerry Sado[2], Senior Member, IEEE, Austin R.J. Downey[1,3], Member, IEEE, Jamil Khan[1], Member, IEEE, and Enrico Santi[2], Senior Member, IEEE,

[1]Dept. of Mechanical Engineering, University of South Carolina, Columbia, SC 29208 USA
[2]Dept. of Electrical Engineering, University of South Carolina, Columbia, SC 29208 USA
[3]Dept. of Civil and Environmental Engineering, University of South Carolina, Columbia, SC 29208 USA

Corresponding author: Kerry Sado (email: ksado@email.sc.edu).

This material is based upon work supported by the Office of Naval Research (ONR) under contract numbers N00014-22-C-1003, N00014-23-C-1012, and N00014-24-C-1301. Approved, DCN# 2026-2-23-2011. DISTRIBUTION STATEMENT A. Approved for public release: distribution is unlimited. "The views expressed are those of the author and do not reflect the official policy or position of the Department of Defense or the U.S. Government."

ABSTRACT Power electronic systems in autonomous vehicles and mission-critical applications are highly susceptible to overheating due to operational inefficiencies. These systems often rely on liquid cooling loops to maintain safe temperatures. However, blockages in cooling loops can lead to temperature rises, component degradation, and eventual system failure. This paper presents a digital twin (DT) approach that enables early detection of coolant-loop blockages and provides a framework for developing autonomous rectification of cooling loop blockages using only temperature sensors. The proposed method integrates transient and steady-state thermal models to detect anomalies and predict system behavior in real-time. A robust detection logic, comprising five independent threshold-based switches, identifies deviations from normal behavior while avoiding false positives. Experimental validation is conducted using a physical testbed to evaluate performance under varying blockage conditions. The system detects blockages in less than 1 min, with temperatures remaining roughly $25\,^{\circ}\mathrm{C}$ below the maximum operating temperature of $80\,^{\circ}\mathrm{C}$, well within safe operating limits. This approach eliminates the need for additional sensing hardware and is well suited to embedded and remote applications.

INDEX TERMS Digital Twin, Blockage Detection, Cooling System, Power Electronics, Decision Making.

I. INTRODUCTION

AUTONOMOUS vehicles (AVs) are increasingly utilized in private, commercial, industrial, and military applications to minimize or eliminate human interaction in hazardous or challenging conditions. Many AVs are partially or fully electric vehicles (EVs), necessitating advanced power electronic systems, such as power converters that inherently generate significant heat due to operational inefficiencies.

Electronic systems are highly sensitive to temperature fluctuations; exceeding temperature thresholds can critically impact performance and reliability, accelerate component degradation, and contribute to approximately 55% of electrical device failures [1]. Even minor temperature variations within acceptable limits can cause undesirable performance deviations and cumulative component degradation over time. Hence, precise temperature monitoring and control through integrated temperature sensors are essential for maintaining system stability, reliability, and longevity. To address this issue, integrated temperature sensors are commonly embedded in power electronic components to enable real-time thermal monitoring. Thermal management for power electronics commonly relies on air cooling or liquid cooling. Air cooling is simple and widely used; however, it offers limited thermal capacity compared to liquid cooling, especially for high-power components [2]. Liquid cooling is thus the preferred method in high-voltage power electronic applications. Various liquid cooling techniques have been investigated, including immersion and spraying, which provide superior heat transfer. Nevertheless, piped coolant systems and heat exchangers are more widely used because of their simpler design, fewer operational constraints, and recent advances in heat exchanger technology, materials, and assembly [3].

Despite their effectiveness, liquid cooling systems remain vulnerable to fluid blockages. In this work, blockages are defined as persistent and unwanted restrictions to fluid flow within piping systems, and may be referred to as restrictions,

flow reductions, or cooling system foulings. In any piping system blockages can be produced by obstruction to the fluid flow and can occur in varying levels of fluid flow reduction. There are methods to reduce the risk of blockages being formed in a system, such as using filters; however, it is nearly impossible to completely remove this risk in practical applications. Thus, it is vital that a system relying on liquid cooling be capable of detecting blockages when they form. The capability of a system to detect a cooling loop blockage before it produces critical temperatures in the affected system is essential for the continued and prolonged use of that system. This is of great concern to AVs in particular, as they are often intended for long, unmanned missions in which a critical system failure would likely result in the loss of the AV and the failure of the mission.

Detecting a cooling loop blockage alone, while useful, does not allow for a system to continue operation. Autonomous systems must also be capable of rectifying blockages to continue operation. Self-healing strategies may include automatically clearing the blockage, rerouting power away from affected modules, or redirecting coolant flow around the blocked location. Such autonomous detection and response requires real-time monitoring, intelligent fault diagnosis, decision making, and control. This blockage detection, and decision making can be accomplished through the use of Digital Twin (DT) technology. A DT is a virtual representation that is dynamically updated with data from its physical counterpart, has predictive capability, and informs decisions [4]. In this work, telemetry from the Physical Twin (PT) updates the model in real-time, and the resulting diagnostic recommendations are acted upon by a human in the loop. The operator serves as the decision-making component that translates model outputs into adjustments on the hardware (e.g., power or flow changes), thereby providing bidirectionality while preserving operator authority. The same decision logic can be integrated into an application layer to enable automated closed-loop control in future deployments, consistent with established views of the digital-twin paradigm and characteristics discussed in [5]–[7] and recent DT-enabled real-time monitoring/control frameworks [8].

Digital Twins were first introduced in 2003, and are generally considered as a digital equivalent to a physical entity [9]–[11]. However, this definition more closely refers to a cybermodel or virtual representation of a physical entity [12]. Digital Twin technology allows for real-time interaction between sensor data and physical systems [13], [14]. In practice, a DT is a virtual model of a physical component or system that integrates real-time sensor data to allow for simulation, prediction, performance optimization, or other procedures using communication to and from the physical component or system [15]–[17]. A properly developed DT must be a faithful representation of its respective physical component or system. In this work, ‘‘faithful” means calibrated to reproduce the PT’s nominal, healthy operating envelope under the same inputs and boundary conditions; departures between PT measurements and the DT’s predicted healthy response are treated as fault signatures. Achieving an accurate representation is generally accomplished through analytical and data-driven characterization or calibration of the DT and/or the respective physical component it is intended to model [18]. Proper calibration allows for the DT to accurately model the performance and function of its physical mirror, referred to as the Physical Twin. Once calibrated, the DT found in this work will utilize temperature sensors commonly embedded within power electronic components, allowing precise modeling of thermal responses for predictive and preventive maintenance [19], [20].

Historically, DTs have proven their effectiveness to optimize, monitor, and predict system health and operational performance across various domains [21], [22]. In aerospace applications, DTs have been used by the National Aeronautics and Space Administration (NASA) and other organizations to monitor air-frame health for aircraft and spacecraft in different operating conditions [23]–[25]. Machining processes for aerospace components have also included DT technology for better autonomous management [26]. General Electric (GE) and Siemens have developed DTs for use in industrial manufacturing applications [27], [28]. Digital Twin technology has been implemented recently by the United States Navy for use in naval operations and shipbuilding procedures [29]–[31]. Recently, the authors demonstrated the use of DT for thermal management of simulated electronic systems, successfully implementing blockage detection capabilities [32].

A range of blockage detection strategies have been proposed for other domains. In oil and gas pipelines, blockages have been detected using computational fluid dynamics (CFD) and comparison of predicted and measured flow profiles [33]. Other approaches include triboelectric nanogenerators for leak detection [34], pressure wave analysis for internal pipe geometry reconstruction [35], and acoustic wave propagation for blockage localization [36]. Additional methods employ liquid level monitoring in sewage systems [37], acoustic sensing combined with neural networks [38], pressure pulse attenuation [39], and frequency response analysis [40], [41].

While effective in their fields, these existing blockage detection methods do not address the specific constraints of power electronic cooling systems and often require custom instrumentation, invasive measurements, or offline analysis. In pipeline-oriented diagnostics, frequency-response and inverse-transient methods can detect and sometimes locate partial or extended blockages; however, they typically require modification to allow the addition of pressure/flow transducers, and deliberate transient excitation (e.g., rapid valve actions or injected pressure waves), with analysis commonly performed offline [40]–[42]. Acoustic approaches including high-frequency acoustic/transient-wave techniques and acoustic reflectometry depend on specialized transducers and non-trivial signal processing and are frequently deployed as scheduled inspections rather than continuously [43], [44]; recent LFM-based implementations likewise require dedicated acoustic hardware [45]. A survey inventories these

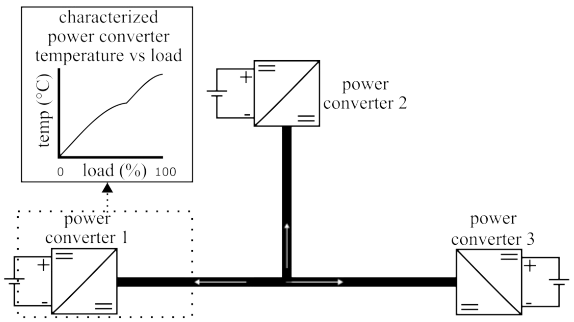

FIGURE 1. Power system under study, consisting of three parallel converter modules delivering power to a DC bus. Each converter is thermally managed by an independent liquid-cooling loop with inlet and outlet manifolds. This configuration forms the basis for the digital twin used to detect coolant blockages using only temperature sensor data.

method families and discusses deployability and instrumentation trade-offs [46].

The installation of pressure transducers or flow meters to an existing system requires inline piping modifications and planned downtime; similarly, many acoustic/frequency-response approaches are inspection-oriented with post-processing, which implies partial or total system deactivation for reliable execution. In 2024, a foundation was developed for the detection of blockage formation in water-cooled power electronics using a digital shadow [47]. While this work addresses the specific constraints of liquid-cooled power electronics, it does not provide embedded real-time operation and focuses on modeling behavior under blocked conditions rather than continuous detection. Therefore, this paper presents a novel digital twin-based approach to blockage detection designed for liquid-cooled power electronic systems that uses only temperature sensors, which are typically pre-installed on many power electronic components. The contributions are twofold. First, an integrated DT combining transient and steady-state thermal models in real-time for rapid and accurate blockage detection is introduced. Second, experimental validation on a realistic physical testbed demonstrates blockage detection within $1\,\mathrm{min}$ while maintaining safe system temperatures.

II. PHYSICAL TWIN ARCHITECTURE

The system under study consists of three parallel power converter modules delivering power to a DC bus, as shown in Figure 1. Each module is thermally managed by a dedicated liquid-cooling loop, consisting of inlet and outlet manifolds. This physical configuration supports the development of a DT capable of detecting and mitigating coolant blockages in real time by relying solely on temperature sensor data, as introduced in Section I. The physical testbed, shown in Figure 2, was specifically designed to emulate the thermal behavior of a system consisting of three parallel power converter modules, as depicted in Figure 1. In this work, this testbed will be referred to as the PT. The PT replicates converter thermal dynamics using three discrete heater elements, each bonded to an aluminum heat exchanger with thermally conductive adhesive to represent the heat sinks found in commercial

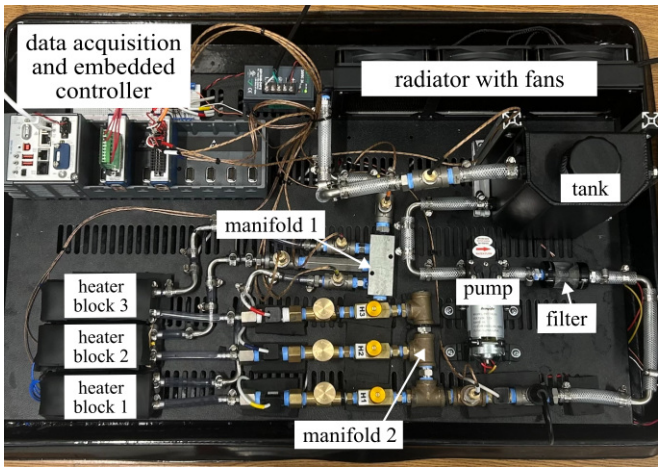

FIGURE 2. The experimental Physical Twin testbed designed to emulate a liquid-cooled power electronics system. Key components include three heater modules (bottom left), a pump and filter (bottom right), a radiator (top right), and the data acquisition/digital twin hardware (top left).

power electronics. Each heater–heat sink pair forms a module, referred to as a heater block. The cooling system is implemented as a closed-loop fluid circuit that includes a pump, radiator, fluid reservoir, and inline filter. The cooling fluid in use is a mixture of 40% propylene glycol by weight with deionized water and a corrosion inhibitor. Proportional control valves are placed at the inlet manifold to emulate partial or complete flow blockages, enabling controlled validation of the blockage detection strategy developed in the DT.

The data acquisition system is built around a National Instruments CompactRIO (cRIO-9035) platform. It interfaces with pressure, temperature, and flow sensors installed at key locations in the system, as shown in Figure 3. Although flow and pressure sensors were utilized during system characterization and calibration phases, blockage detection was performed exclusively using temperature measurements from surface mount, k-type, stick-on thermocouple sensors affixed to the heater modules [48]. The temperature measurement uncertainty is determined from the thermocouple and acquisition specifications (accuracy and response time per manufacturer datasheet and DAQ configuration), and this uncertainty contributes directly to the PT-DT residual used for detection. Later, the developed DT was deployed at a sampling rate of 1 Hz on the cRIO-9035, which was responsible not only for data acquisition but also for executing the DT models and detection logic in real time. This setup enabled continuous temperature data analysis and autonomous identification of coolant blockages within the physical system.

III. DIGITAL TWIN SYSTEM OVERVIEW AND DEVELOPMENT

As shown in Figure 4, the DT-enabled detection framework ingests Physical Twin (PT) temperature measurements and power commands, computes diagnostic indicators in the digital model, and outputs a blockage status for operator action; the two core modules are: the digital model (transient + steady-state) and the detection logic. Telemetry from the PT

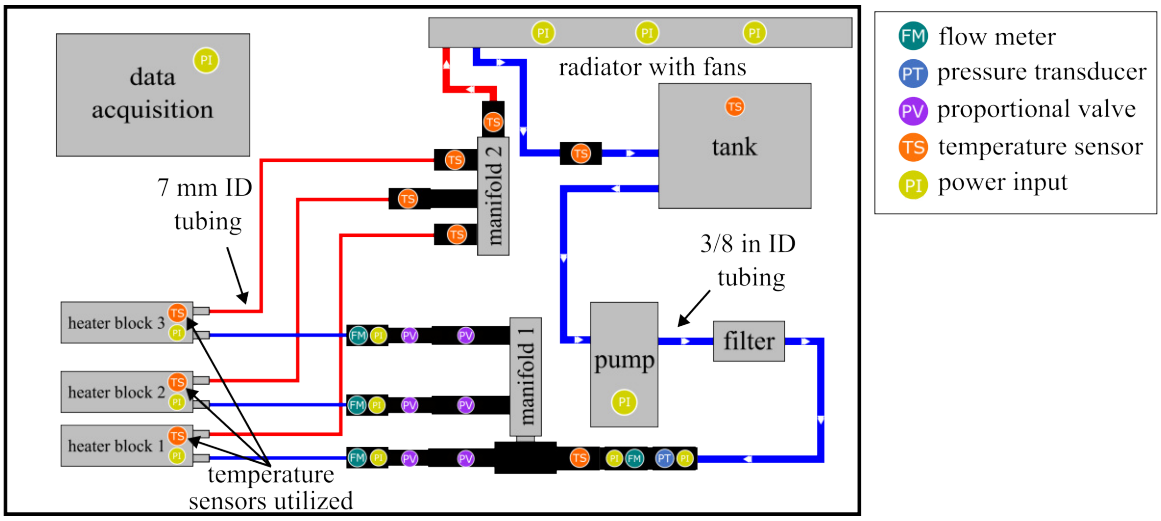

FIGURE 3. **A schematic of the Physical Twin testbed, illustrating the parallel coolant flow paths to the three heater modules, sensor locations (flow, pressure, temperature), and power input locations. While the system includes various sensors for general system monitoring, only the highlighted temperature sensors were used for the tests conducted in this paper.**

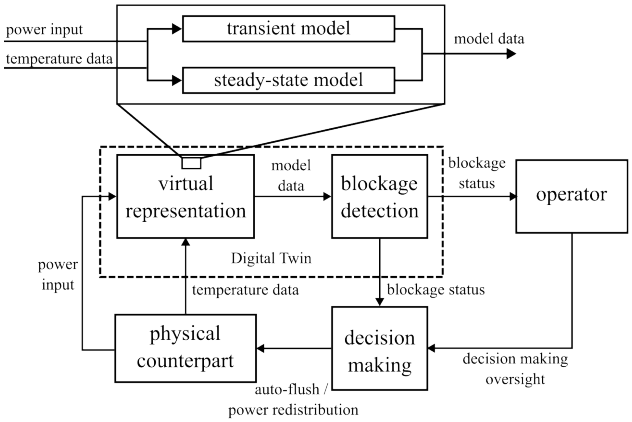

FIGURE 4. **System architecture of the digital twin. The DT receives power and temperature data from the physical twin, which it processes using real-time transient and steady-state models to perform blockage detection and enable decision-making. Bidirectionality is currently provided by a human in the loop who applies recommended power or flow adjustments; the same pathway is automatable.**

updates the model in real-time, and the return path is human-in-the-loop. The operator serves as the decision-making component, translating model recommendations into adjustments on the hardware (e.g., power or flow changes). This provides bidirectionality while preserving operator authority; the same decision logic can be integrated into an application layer to enable automated closed-loop control in future deployments.

A. DIGITAL MODEL

The digital model comprises a transient thermal model and a steady-state temperature model that run in real time at 1 Hz on the NI cRIO-9035. These models are designed to be computationally light to allow for real time operation on standard NI hardware. The transient model is a calibrated physics-based reconstruction of the PT. Given power inputs and environmental measurements, it simulates the healthy thermal response of the PT and produces real-time temperature estimates that match the system under the same inputs and boundary conditions. The steady-state model computes an instantaneous healthy-state bound that is used for fast cross-checks. Figure 4 shows the overall DT–PT integration and Figure 5 summarizes how these model outputs are consumed by the detection logic. Both models are consistent with Fourier's law of conduction in (1) and Newton's law of cooling in (2). The symbols used in those relations are listed in Table 1. The specific model instantiations used for simulation and detection are given in the following.

$$q = -k \cdot \nabla T \tag{1}$$

$$q = h_c \cdot A \cdot dT \tag{2}$$

TABLE 1. **Variables used in equations** (1) **and** (2)**.**

Variable Name	Symbol
Heat Flux	q
Heat Conduction Coefficient	k
Temperature Gradient	∇T
Heat Convection Coefficient	h_c
Heat Exchanger Surface Area	A
Infinitesimal Temperature Difference	$\mathrm{d}T$

Transient model: Each cooled module $i = 1, \ldots, N$ is represented as a thermal mass C_i with temperature T_i. The coolant manifold is represented by well-mixed one-dimensional segments with temperatures $T_{f,s}$ and volumes V_s. Measured or commanded inputs are the module powers P_i, the mass flow $\dot{m}$, the inlet fluid temperature $T_{f,\mathrm{in}}$, and the ambient temperature T_∞. The module energy balance is

$$C_i \frac{dT_i}{dt} = P_i - h_i A_i \left(T_i - T_{f,\sigma(i)}\right) - \sum_{j \in \mathcal{N}(i)} k_{ij} \left(T_i - T_j\right), \tag{3}$$

where $h_i A_i$ is the effective convection conductance to the adjacent fluid segment $\sigma(i)$ and k_{ij} are lumped conductive couplings to neighboring modules $\mathcal{N}(i)$. The fluid energy balance for segment s is

$$\begin{aligned} \rho c_p V_s \frac{dT_{f,s}}{dt} + \dot{m} c_p \left(T_{f,s} - T_{f,s-1}\right) \\ = \sum_{i \in \mathcal{M}(s)} h_i A_i \left(T_i - T_{f,s}\right) \quad - U_w A_{w,s} \left(T_{f,s} - T_\infty\right) \end{aligned} \tag{4}$$

with ρ and c_p the fluid density and heat capacity, $U_w A_{w,s}$ a wall-to-ambient conductance, and $\mathcal{M}(s)$ the set of modules exchanging heat with segment s. For $s = 1$, the upstream temperature is $T_{f,0} = T_{f,\mathrm{in}}$. Boundary conditions are imposed via the measured inlet coolant temperature ($T_{f,0} = T_{f,\mathrm{in}}$) and the measured ambient temperature (T_∞). Assumptions include incompressible single-phase flow, one-dimensional advection, and well-mixed nodes so the model executes deterministically at 1 Hz for the seconds-to-minutes detection time scale. The Simscape implementation uses Thermal Mass, Temperature Source, Heat Flow Rate Source, Conductive Heat Transfer, and Convective Heat Transfer blocks, which implement the balances in (3) and (4).

Solver and discretization: The network is integrated with an implicit backward-Euler scheme with step $\Delta t = 1\,\mathrm{s}$ synchronized to the sensor stream. For module i, (3) leads to

$$\left(\frac{C_i}{\Delta t} + h_i A_i + \sum_{j \in \mathcal{N}(i)} k_{ij}\right) T_i^{k+1} - \sum_{j \in \mathcal{N}(i)} k_{ij} T_j^{k+1} - h_i A_i T_{f,\sigma(i)}^{k+1} = \frac{C_i}{\Delta t} T_i^k + P_i^k. \tag{5}$$

and for fluid segment s, (4) gives

$$\left(\frac{\rho c_p V_s}{\Delta t} + \dot{m} c_p + U_w A_{w,s} + \sum_{i \in \mathcal{M}(s)} h_i A_i\right) T_{f,s}^{k+1} - \dot{m} c_p T_{f,s-1}^{k+1} - \sum_{i \in \mathcal{M}(s)} h_i A_i T_i^{k+1} = \frac{\rho c_p V_s}{\Delta t} T_{f,s}^k + U_w A_{w,s} T_\infty^k. \tag{6}$$

At each 1 Hz cycle the linear system formed by (5) and (6) is solved to obtain $\{T_i^{k+1}, T_{f,s}^{k+1}\}$. Initial conditions are the measured temperatures at model start.

Steady-state model: In parallel, the steady-state branch computes an instantaneous healthy-state bound for comparison

$$T_{ss}(t) = T_\infty(t) + \frac{P(t)}{hA}, \tag{7}$$

where $P(t) = \sum_i P_i(t)$. The aggregate conductance hA is identified from healthy calibration data by fitting steady-state temperature versus power. When per-module parameters are available the per-module form $T_{ss,i} = T_\infty + P_i/(h_i A_i)$ is used. This bound is referenced by the detection logic shown in Figure 5 as the physical-limit check.

Runtime interface with detection: At each second the PT provides $T_{f,\mathrm{in}}$, T_∞, $\dot{m}$, and $\{P_i\}$ to the model. The outputs $\{T_i^{\mathrm{DT}}\}$ and $\{T_{f,s}^{\mathrm{DT}}\}$ are compared with PT temperatures to form residuals and features used by the five-switch detection logic described in the following subsection and summarized in Figure 5.

B. BLOCKAGE DETECTION

Since the DT is designed to be a faithful representation of the PT under standard, healthy operational conditions, the blockage detection algorithm is able to compare temperature data from the PT against the healthy temperature data provided by the DT. This comparison is executed through five independent logic procedures, each implemented as a binary switch. Every switch outputs a high signal when a specific discrepancy is detected and a low signal when no anomaly is present. Each is tailored to identify a distinct thermal behavior pattern associated with coolant blockages, contributing to a comprehensive and robust detection mechanism. These switches are outlined in Figure 5 and are explained in detail in the following.

1) **Temperature Inconsistency Switch 1** compares the real-time simulated temperature from the DT (T_{DT}) with the measured temperature from the PT (T_{PT}). When the absolute difference between the two values exceeds a predefined threshold ϵ_{T1}, the switch transitions to a high state, indicating abnormal thermal behavior. The condition is expressed as

$$|T_{\mathrm{PT}}(t) - T_{\mathrm{DT}}(t)| > \epsilon_{T1} \tag{8}$$

2) **Temperature Inconsistency Switch 2** introduces an additional layer of filtering to reduce false-positive detections. It follows the same logic as Switch 1 but applies a higher threshold ϵ_{T2}. Switch 2 applies a higher residual threshold and a longer persistence window to the same PT–DT temperature residual used by Switch 1. Together they act as a sensitivity–specificity pair; Switch 1 serves as an early indicator, while Switch 2 requires a larger, sustained deviation before contributing to the final decision. The corresponding condition is

$$|T_{\mathrm{PT}}(t) - T_{\mathrm{DT}}(t)| > \epsilon_{T2} \tag{9}$$

3) **Temperature Change Derivative Switch** evaluates the rate of temperature variation to assess the likelihood of a blockage. It calculates the time derivative of the temperature measurements from both the PT and the DT, then compares their difference to a predefined threshold $\epsilon_{\frac{dT}{dt}}$. Blocked coolant paths typically exhibit rapid heating and delayed cooling, deviating from the expected thermal profile. This behavior is illustrated in Figure 6. The detection logic is defined as

$$\frac{dT}{dt} = \frac{T(t) - T(t - \Delta t)}{\Delta t} \tag{10}$$

$$\left|\left(\frac{dT}{dt}\right)_{\mathrm{DT}}(t) - \left(\frac{dT}{dt}\right)_{\mathrm{PT}}(t)\right| > \epsilon_{\frac{dT}{dt}} \tag{11}$$

Because this switch uses derivative information, it is sensitive to measurement noise and therefore performs

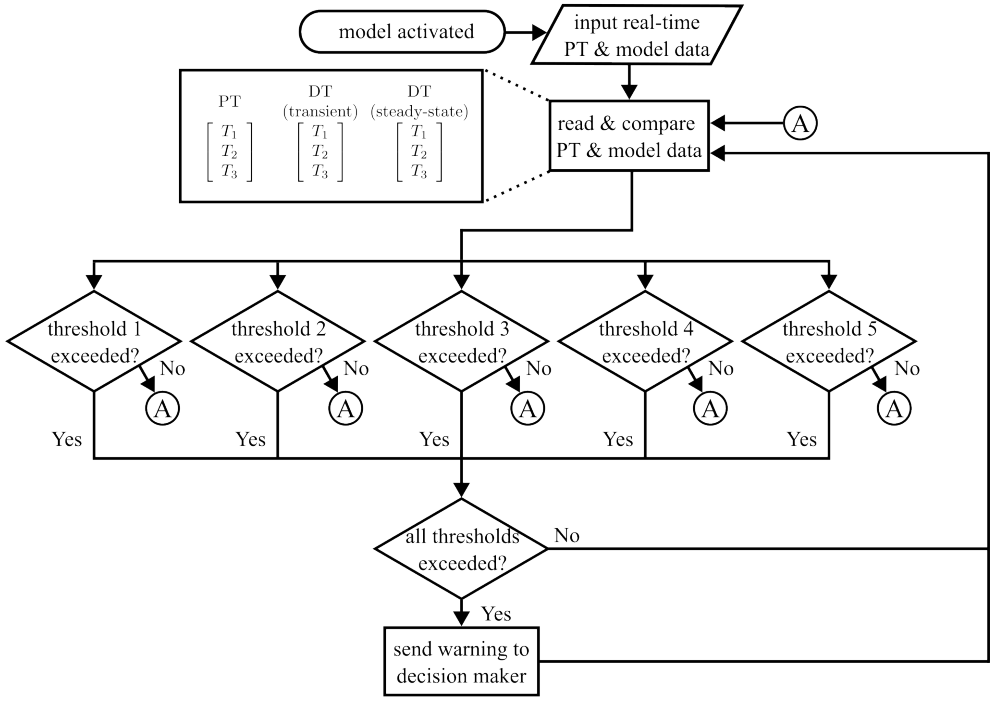

FIGURE 5. **Detailed logic of the blockage detection module. The system continuously compares real-time data from the Physical Twin (PT) with data from the transient and steady-state digital models. A blockage warning is triggered only if the discrepancies exceed all five predefined thresholds, ensuring a robust detection mechanism.**

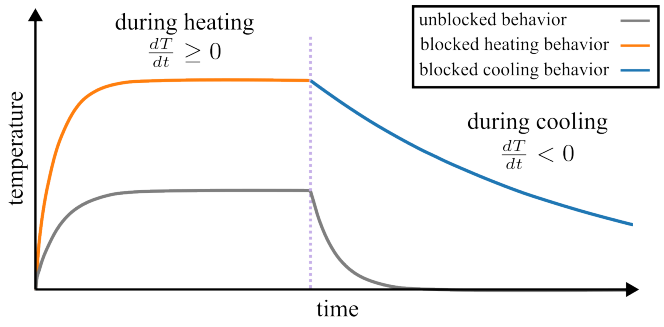

FIGURE 6. **Characteristic thermal signatures of a liquid-cooled system. Compared to normal (unblocked) behavior, a blocked cooling line causes temperatures to rise more rapidly during heating and cool more slowly once the heat source is removed. This distinct change in the temperature's rate of change (dt/dT) is a key indicator used for detection.**

more effectively when thermal data is partially filtered. Despite this sensitivity, it serves as an early indicator of emerging blockages in the cooling loop.

4) **Inter-Module Comparison Switch** examines temperature disparities between modules to identify flow redistribution caused by a blockage. In a system with constant volumetric flow, the total coolant flow rate, Q_{Total}, is the sum of the flow through each module

$$Q_{\text{Total}} = Q_1 + Q_2 + Q_3 + ... + Q_n \tag{12}$$

For the system under study with three modules, this becomes

$$Q_{\text{Total}} = Q_{\text{M1}} + Q_{\text{M2}} + Q_{\text{M3}} \tag{13}$$

If a blockage forms in one module, its coolant flow rate decreases while the other modules compensate by drawing more flow. This redistribution leads to elevated temperatures in the blocked module and unexpectedly lower temperatures in the unblocked ones, disrupting the inter-module thermal balance. An illustration of this temperature shift is shown in Figure 7. When a blockage occurs (e.g., in Heater 1), the reduced flow causes a temperature rise in that module. Simultaneously, increased coolant flow to neighboring modules lowers their temperatures relative to the digital twin's predictions. The detection logic identifies abnormal behavior by comparing the measured inter-module temperature differences in the PT to expected values from the DT. If the discrepancy exceeds a defined threshold, the system switch transitions to a high state, signaling a potential blockage.

$$|(\Delta T_{\text{M1}-\text{M2}})_{\text{PT}} - (\Delta T_{\text{M1}-\text{M2}})_{\text{DT}}| > \epsilon_{1-2} \tag{14}$$
$$|(\Delta T_{\text{M1}-\text{M3}})_{\text{PT}} - (\Delta T_{\text{M1}-\text{M3}})_{\text{DT}}| > \epsilon_{1-3} \tag{15}$$
$$|(\Delta T_{\text{M2}-\text{M3}})_{\text{PT}} - (\Delta T_{\text{M2}-\text{M3}})_{\text{DT}}| > \epsilon_{2-3} \tag{16}$$

This switch enhances system robustness and is effective when at least one module remains unaffected, as it enables detection of both single and multiple blockages based on relative module temperatures.

5) **Steady-State Bound Switch** compares the instantaneous PT temperature with the healthy steady-state bound computed from Eq. (7) for the current power

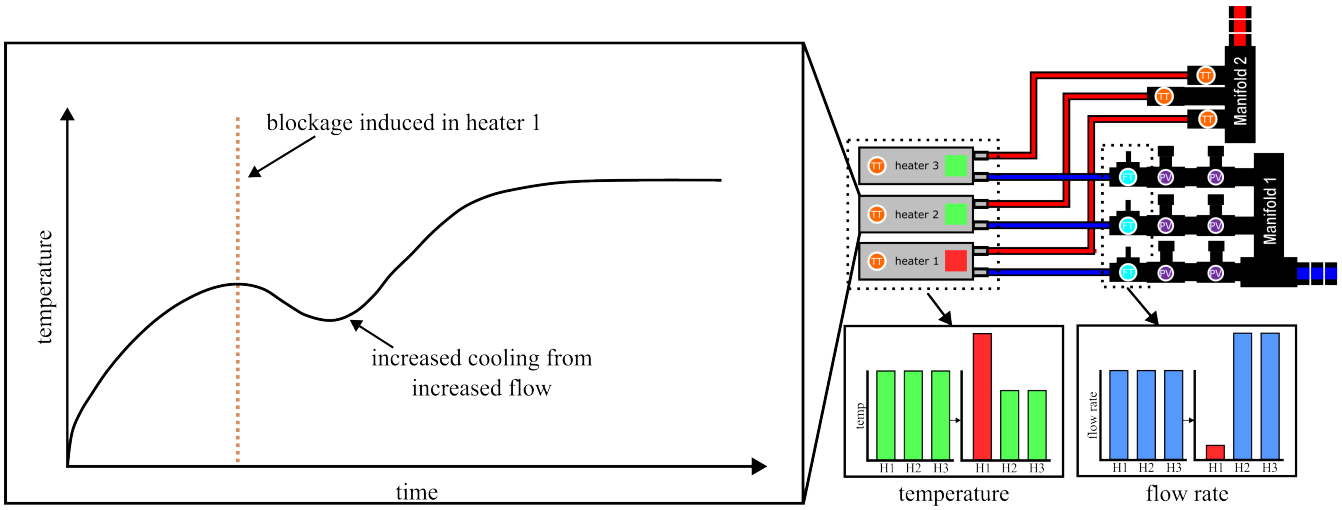

FIGURE 7. Illustration of the inter-module temperature effect used for blockage detection. When a blockage occurs in one module (e.g., Heater 1), its coolant flow is reduced, causing a temperature increase. This redirects coolant to neighboring unblocked modules, proportionally increasing their flow rate and causing their temperatures to drop unexpectedly relative to the model's prediction.

and ambient conditions. The check is evaluated every second and does not require the PT to be at steady state. If the PT temperature persistently exceeds the bound by a small margin (thresholds from healthy baselines; see Section III-B), the switch asserts. This provides a fast, physics-based upper-limit test that complements the transient residual, derivative, and inter-module checks and helps suppress false positives. A significant overshoot may suggest flow restriction. Conversely, during cooling, the PT temperature should approach the predicted lower steady-state temperature.

The switch behavior depends on whether the system is heating or cooling, as determined by the sign of the temperature derivative.

$$\frac{dT}{dt} \geq 0 : |T_{\mathrm{ss-PT}} - T_{\mathrm{ss-DT}}| > \epsilon_{\mathrm{ss-heating}} \quad (17)$$

$$\frac{dT}{dt} < 0 : |T_{\mathrm{ss-PT}} - T_{\mathrm{ss-DT}}| > \epsilon_{\mathrm{ss-cooling}} \quad (18)$$

The switching thresholds are set using the DT steady-state prediction and predefined tolerance margins:

$$\epsilon_{\mathrm{ss-heating}} = T_{\mathrm{ss-DT}} + N_{\mathrm{heating}} \quad (19)$$

$$\epsilon_{\mathrm{ss-cooling}} = T_{\mathrm{ss-DT}} - N_{\mathrm{cooling}} \quad (20)$$

This logic allows the switch to adapt to both thermal rising and falling conditions. When the measured steady-state temperature deviates excessively from the DT prediction, the switch transitions to a high state, indicating a potential blockage. The adaptive design of this switch enhances detection accuracy and minimizes false positives in dynamic thermal environments.

Each of the switches used in the blockage detection model serves a specific purpose, and utilizes customizable thresholds to adapt to various applications and safety requirements. Additionally, as this system is modular, the implementation of a digital twin for any use in liquid-cooling blockage detection may include or exclude any combination of the previously defined switches. This allows for significant customization, which solidifies this technology as a versatile method of detecting blockages in liquid-cooling loops. Furthermore, the system as presented in this work requires all switches to be activated before detecting a blockage, as shown in Figure 5. However, the modularity of the system also allows for any combination of the included switches to require activation before a blockage is flagged. This allows for the detailed selection of switches and activation configurations for individual system-specific use cases. The switch and activation configuration used for the simulated and experimental test cases found in this paper was chosen to minimize the risk of false positives, while other possible configurations may slightly increase the rate at which false positives occur to provide more rapid blockage detection. The values used for each switching threshold are system specific, determined by the operators based on results from preliminary testing. The values used by the authors in the following simulated and experimental tests can be found in Table 2.

Some approaches may consider comparison with a constant temperature limit. However, a single constant limit on a PT temperature will not signal until the PT has already heated substantially, and it has no knowledge of the expected steady-state temperature at the present power and ambient temperature. As a result, such a rule tends to detect late at low ambient or low power and to raise false alarms during hot ambient or commanded power steps. The DT conditions its expectations on the current inputs each second; residual and dynamics-based tests (Switches 1–4) can indicate anomalies even when absolute temperatures are low, and the steady-state bound in Eq. (7) scales with power and ambient to provide a physical upper limit. Advisory warnings from individual

switches are possible, whereas a blockage is confirmed only when all five switches are active for a short dwell, as shown in Figure 5.

TABLE 2. Epsilon values used in blockage detection algorithm for simulations and experimental testing.

Switch Name	Symbol	Value
Temp Difference 1	ϵ_{T1}	$0.75\,^{\circ}\mathrm{C}$
Temp Difference 2	ϵ_{T2}	$1.00\,^{\circ}\mathrm{C}$
Rate of Change	$\epsilon_{\frac{dT}{dt}}$	$0.125\,^{\circ}\mathrm{C\,s^{-1}}$
Inter-Module	ϵ_{IM}	$1.50\,^{\circ}\mathrm{C}$
Steady-State	ϵ_{ss}	$0.40\,^{\circ}\mathrm{C}$

IV. INITIAL SIMULATION RESULTS

Prior to running the physical and digital twins in parallel through experimental testing, a comprehensive simulation study was conducted to evaluate the performance of the proposed DT framework. A detailed model of the PT, incorporating thermal and fluid dynamics, was created in MATLAB Simscape to emulate realistic system behavior under various operating and fault conditions.

This simulated PT model was operated alongside the DT in a synchronized simulation environment. The DT received simulated inputs concurrently with the simulated PT and used its internal models to predict system behavior for comparison. Both models executed faster than wall-clock time, which enabled rapid validation of the detection logic before hardware experiments. Three representative use cases were simulated to assess the effectiveness of the blockage detection approach.

A. SIMULATED TEST 1: RAPID SINGULAR FULL FOULING

The first simulated case, illustrated in Figure 8, evaluates the DT response to a sudden and severe blockage in one module. A 99% flow restriction was applied to Heater Block 3 (HB3) at $t = 60\,\mathrm{min}$. A complete blockage was not simulated due to solver convergence limitations in the model. After the blockage event, HB3 exhibited a rapid and sustained thermal increase compared to the other modules. This deviation was successfully captured by the DT detection logic. The blockage was detected within $10\,\mathrm{min}$ of onset, demonstrating the DT capability to identify critical thermal anomalies under fast-developing fault scenarios.

B. SIMULATED TEST 2: RAPID DUAL FULL FOULING

The second simulated case further demonstrates the capability of the DT system to detect multiple simultaneous faults. Similar to the first case, this test introduces a 99.5% blockage in both Heater Block 1 (HB1) and Heater Block 3 (HB3) at $t = 60\,\mathrm{min}$. Note that while HB1 and HB3 experience a smaller temperature increase than expected due to a limitation in MATLAB Simscape, their temperatures do begin to increase more rapidly as a result of the blockage. As expected,

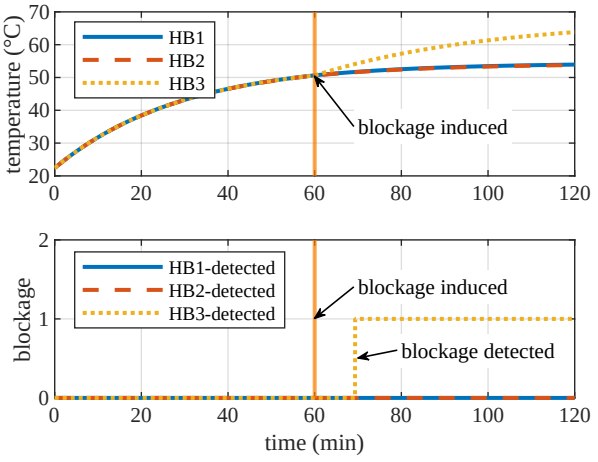

FIGURE 8. Simulation results for a rapid 99.5% blockage induced in Heater Block 3 (HB3) at $t = 60$ min. The top plot shows the temperature divergence of HB3, while the bottom plot confirms successful detection by the DT system.

Heater Block 2 (HB2) exhibited increased cooling due to redirected coolant flow from the two restricted channels. This inter-module effect, amplified by dual fouling, resulted in an even more pronounced temperature divergence. Figure 9 illustrates the thermal behavior of all three modules and confirms successful detection of the dual blockage within $15\,\mathrm{min}$.

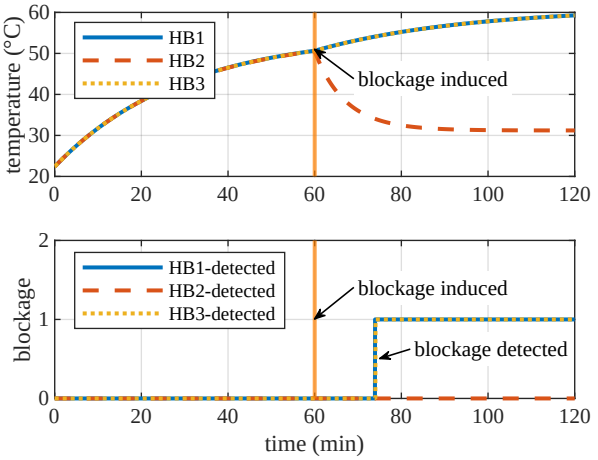

FIGURE 9. Simulation results for a rapid dual blockage induced in Heater Blocks 1 and 3 at $t = 60$ min. The temperatures of the affected modules rise, while the unblocked module (HB2) shows a distinct cooling effect from the increased coolant flow. The system successfully detected the blockage within 20 min.

C. SIMULATED TEST 3: SLOW-ONSET SINGULAR FULL FOULING

The final simulation, shown in Figure 10, evaluated the DT system's ability to detect a gradually forming blockage. In this case, a linear restriction was applied to Heater Block 2 (HB2), increasing from 0% to 99.5% over the span of one hour. The fouling event was initiated at $t = 60\,\mathrm{min}$. The DT detected the abnormal thermal behavior within $25\,\mathrm{min}$ of the onset. This result demonstrates the system's effectiveness in identifying progressive faults prior to the point of complete flow restriction.

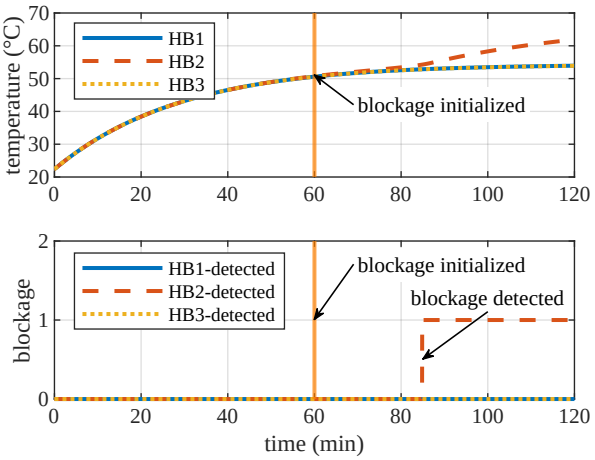

FIGURE 10. Simulation of a gradual blockage applied to Heater Block 2 (HB2), beginning at $t = 60$ min and linearly increasing to 99.5% over one hour. The DT detected the fault within 25 min, confirming its sensitivity to slowly developing faults.

D. SIMULATION CONCLUSIONS

The results of the simulated tests demonstrated the capability of the DT system to detect a range of blockage conditions in liquid-cooling systems with high responsiveness. In the rapid singular blockage case, detection was achieved within $10\,\mathrm{min}$ of induction. When dual blockages were introduced simultaneously, the DT identified the faults within $15\,\mathrm{min}$. In the slow-onset scenario, where the blockage developed gradually over one hour, the system successfully detected the anomaly within $25\,\mathrm{min}$ of initiation, well before reaching critical flow restriction. These timeframes indicate that the DT is capable of identifying both abrupt and progressive failures. However, the time required for detection will depend on the thermal characteristics of the monitored components. Systems with higher thermal mass may exhibit slower temperature dynamics, potentially extending the detection time.

V. EXPERIMENTAL TESTING RESULTS

Following simulation-based validation, experimental evaluations were conducted using the PT testbed shown in Figure 2. These experiments were designed to validate the performance of the DT in online blockage detection under nominal and faulted conditions. With the exception of calibration tests, each distinct testing configuration was tested a minimum of four times to ensure consistent operation of the DT. The results for each test in each distinct configuration were sufficiently similar to the other tests in the same configuration to justify the presentation and discussion of only one data set per experimental testing configuration. For the purposes of this work, real-time means that the DT executes synchronously with the sensor stream at $1\,\mathrm{Hz}$. At each second the system ingests new PT measurements, advances one solver step, computes features, and updates the five switches within the same $1\,\mathrm{sec}$ cycle. Accordingly, computational latency from measurements to blockage-flag update is bounded by the $1\,\mathrm{sec}$ execution period, providing a maximum delay of one-cycle. Consequently, the detection times reported here are dominated by the physical thermal dynamics of the PT and the chosen thresholds rather than computational latency. Other sensing modalities (e.g., pressure or acoustic measurements) can respond faster than temperature but typically require added instrumentation or controlled excitation; our focus is a temperature-only implementation suited to embedded power-electronics platforms. The remainder of this section describes the test procedures and summarizes performance.

A. TEST 1: DT CALIBRATION

The first experimental task involved calibrating the DT to match the thermal response of the PT under nominal conditions. Initially, the DT was configured using thermal parameters derived from manufacturer datasheets and known material properties. Real-time operation of the DT in parallel with the PT allowed direct comparison between simulated and measured thermal behavior without introducing any flow obstructions. As shown in Figure 11, the DT captured the overall temperature trends of the PT, though small discrepancies with Root Mean Squared Error (RMSE) values as high as $2\,^{\circ}\mathrm{C}$ were observed. To improve accuracy, a series of five calibration runs were performed to iteratively adjust key thermal parameters. These refinements enabled the DT to match the PT temperature trajectories within $0.65\,^{\circ}\mathrm{C}$ RMSE, with a typical deviation of $0.2\,^{\circ}\mathrm{C}$, as shown in Figure 12 and detailed in Table 3. The calibrated PT-DT residual statistics (RMSE and typical deviation) provide an empirical bound on combined uncertainty due to sensor noise/lag and model mismatch under healthy operation and serve as the baseline uncertainty level for threshold selection. The resulting DT model integrates physics-based thermal calculations with data-informed tuning, achieving high fidelity under steady-state and transient conditions. This validated thermal consistency between the DT and PT forms the basis for reliable blockage detection in subsequent experiments.

The DT core in this manuscript is physics based, using mechanistic energy-balance equations with calibrated effective parameters; data-driven training approaches (e.g., learned predictors requiring large historical datasets) are outside the scope of this work. Commissioning therefore consists of calibrating effective thermal parameters using a limited amount of healthy-operation data spanning representative operating conditions (power commands and boundary inputs such as $T_{f,\mathrm{in}}$ and T_{∞}). Gradual aging, fouling, or performance degradation is expected to manifest as slow changes in effective conductances (e.g., reduced convection hA) and/or a drift in PT-DT residual bias; when such drift becomes sustained relative to the calibrated healthy residual envelope, a short recalibration run can be used to re-identify the affected conductances and restore the healthy baseline used for detection.

B. TEST 2: RAPID SINGULAR FULL FOULING

Following successful calibration and characterization of the DT against the PT, the first experimental blockage detection scenario was conducted. This test was designed to evaluate the DT's ability to detect a rapidly induced full block-

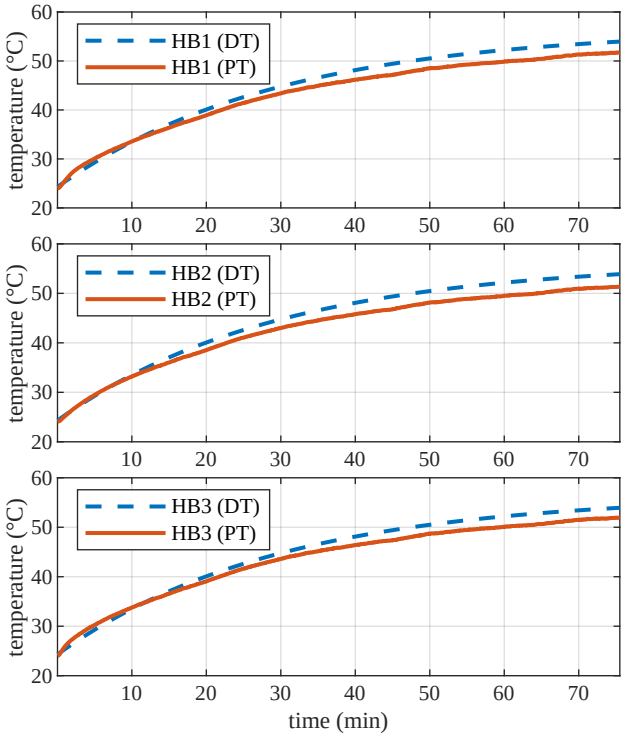

FIGURE 11. **Initial calibration results for the digital twin, using only manufacturer-supplied material properties and data sheets. The plots for all three heater blocks show a significant deviation between the predicted temperature (DT) and the actual measured temperature (PT), highlighting the need for data-driven fine-tuning.**

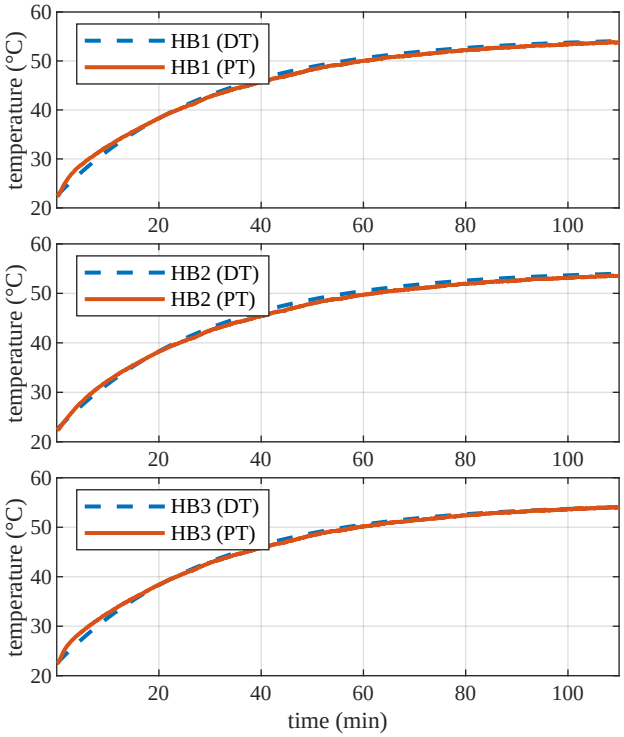

FIGURE 12. **Final calibration results after fine-tuning the DT with experimental data. The model's temperature predictions (DT) now closely track the physical twin's measurements (PT) with a mean deviation under 0.5 °C.**

age in one of the cooling branches. To emulate this condition, the proportional valve controlling the coolant flow to Heater Block 1 (HB1) in the PT was fully closed at $t = 34.5\,\text{min}$. This action simulated a sudden and complete fouling event in the cooling channel associated with one module of a representative power electronics system.

The DT, operating in real time, continuously compared temperature responses from the PT with its internally predicted values. A deviation beyond the configured threshold was observed, and the system identified the anomaly as a blockage. Detection occurred $0.8\,\text{min}$ after the blockage was induced, demonstrating the DT's responsiveness under fast fault conditions. As shown in Figure 13, the thermal deviation stabilized once the operator reopened the valve to emulate fault clearance, leading to recovery of the thermal profile.

TABLE 3. **RMSE values (°C) between DT and PT temperatures for three modules before and after data-driven calibration.**

Heater Block #	Pre-Data RMSE (°C)	Post-Data RMSE (°C)
HB1	1.7434	0.5845
HB2	2.0071	0.6407
HB3	1.5551	0.5114

C. TEST 3: RAPID DUAL FULL FOULING

In this test, blockages were introduced simultaneously in two cooling branches to evaluate detection performance under multiple fault conditions. At $t = 26.5\,\text{min}$, the proportional valves controlling flow to Heater Blocks 2 and 3 (HB2 and HB3) in the PT were fully closed to emulate dual full fouling events. The DT, operating in real time, identified abnormal thermal behavior and triggered a blockage warning $0.97\,\text{min}$ after the blockages were induced. As shown in Figure 14, the DT accurately captured the deviation from expected temperatures, and the alert prompted the operator to reopen the blocked paths. This action restored normal cooling and led to system stabilization, validating the DT's ability to detect concurrent faults across multiple branches.

D. TEST 4: SLOW-ONSET SINGULAR FULL FOULING

The final experimental test evaluated the DT's ability to detect gradually developing blockages over extended periods. In this test, an incremental restriction was initiated in Heater Block 2 (HB2) of the PT at $t = 5\,\text{min}$. The flow was increasingly restricted in equal steps over the next hour. As shown in Figure 15, the blockage reached 95% flow reduction at $t = 59.78\,\text{min}$. Prior to this point, the DT identified abnormal thermal behavior and triggered a warning signal at $t = 59.2\,\text{min}$, demonstrating its ability to detect blockages before reaching critical restriction levels.

For data collection purposes, the induced restriction continued to full flow obstruction after detection. The operator then intervened to restore cooling flow and return the system to

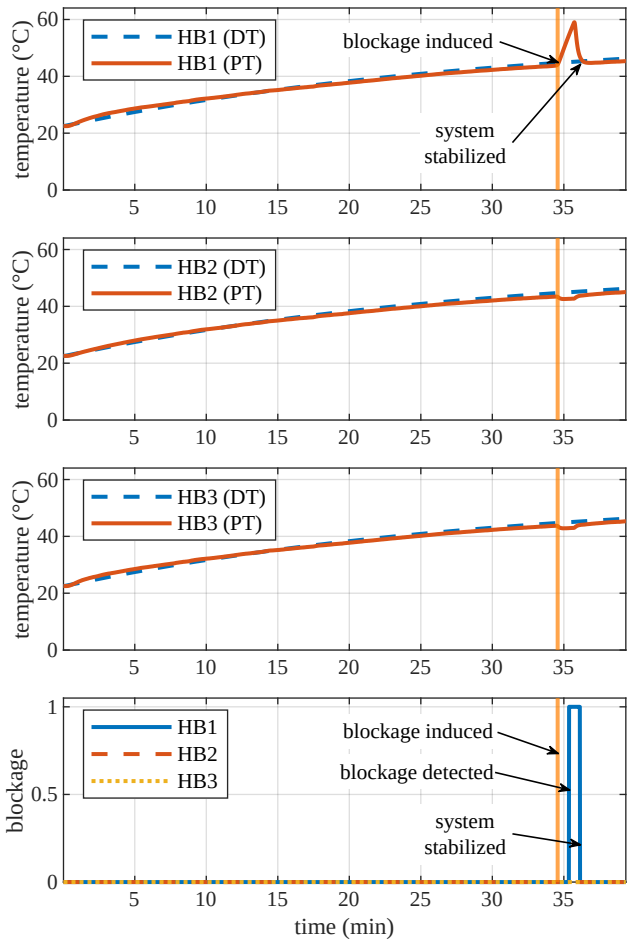

FIGURE 13. **Experimental results for a rapid, total blockage of Heater Block 1 (HB1) at t = 34.5 min. The system detected the fault in 0.8 min, triggering a warning that led to manual system stabilization.**

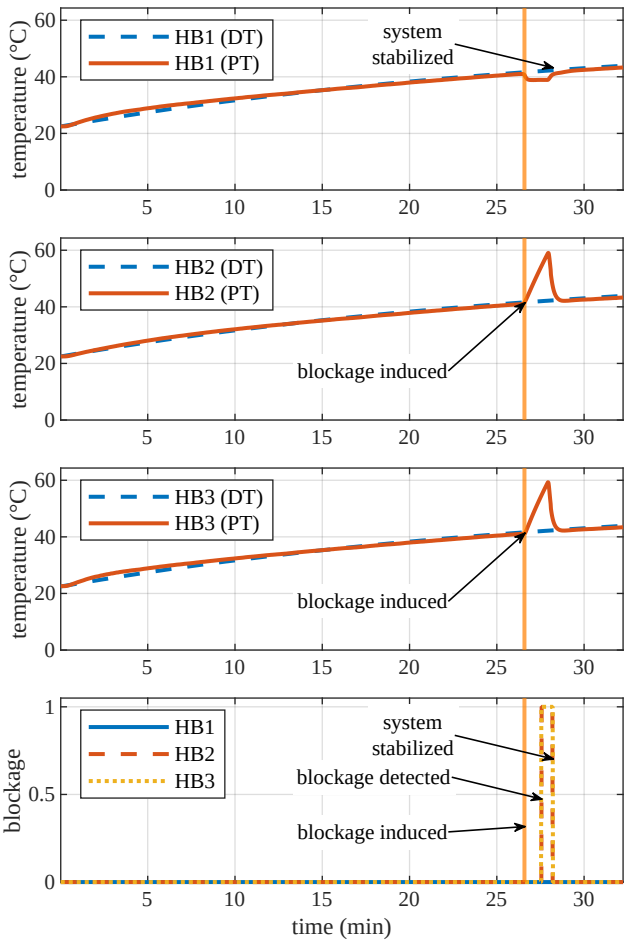

FIGURE 14. **Experimental results for rapid, total, dual-module blockage. The system successfully identified the fault within 0.97 min of induction, demonstrating its ability to detect simultaneous obstructions in multiple modules.**

stable operating conditions. This test demonstrates the DT's sensitivity to slow-onset faults and its effectiveness in early anomaly detection.

E. DISCUSSION OF EXPERIMENTAL RESULTS

The experimental results validate the ability of the DT to detect various cooling system anomalies in real time across both rapid and gradual blockage scenarios. Experimental results held consistent across repeated tests within the same configuration. For fast-developing faults, such as the full blockage in a single or dual module, the DT issued alerts within $1\,\mathrm{min}$ of fault induction. This rapid detection enables timely intervention and minimizes the risk of thermal overstress in power electronic components. In the dual-module test, despite simultaneous disruptions, the DT correctly identified the condition and maintained detection speed and reliability.

The results included in Table 4 denote the maximum temperature of the system at blockage detection as well as a comparison between the maximum temperature at induction and detection. From these metrics, it is seen that blockages tend to be detected by the system at a similar temperature. In each case, the system detected a blockage before the heat increased by more than $14\,^{\circ}\mathrm{C}$. The table also shows the time from induction to detection data, which demonstrates a rapid system response, detecting a blockage in under $1\,\mathrm{min}$ in each test. The final set of data in the table is the ΔT between system maximum and critical temperatures. This data exhibits the capacity of the system to provide warning long before critical temperature levels are reached. The critical temperature for the system in question is $80\,^{\circ}\mathrm{C}$.

In the slow-onset case, the DT detected the blockage before reaching 95% flow reduction, confirming its capability to identify faults that evolve incrementally over longer timeframes. This is particularly valuable for preemptive maintenance in mission-critical systems, where early warnings can prevent system degradation. Across all scenarios, the DT maintained close thermal agreement with the PT due to systematic calibration and iterative refinement. This fidelity is critical for accurate detection performance. The detection accuracy depends directly on how well the DT reflects the physical behavior of the PT. High-fidelity modeling of thermal dynamics, material characteristics, and system configuration enhances the DT's sensitivity to anomalies. Conversely, oversimplified or mischaracterized models can introduce false

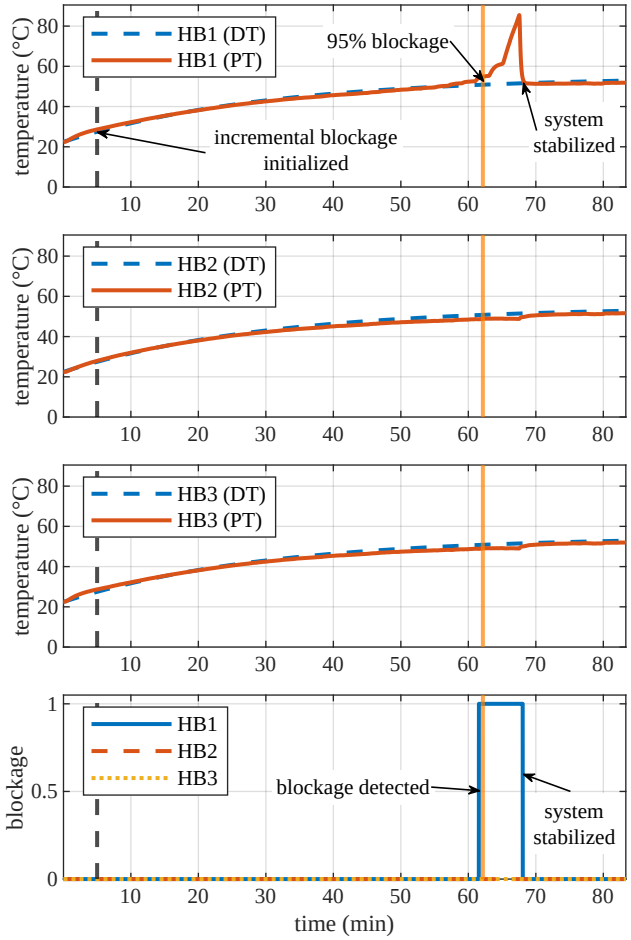

FIGURE 15. **Experimental results for a slow-developing blockage in a single module: Heater Block 1 (HB1). The system detected the extended fault 0.58 min prior to 95% blockage was reached, demonstrating its ability to identify gradual obstructions in individual components.**

TABLE 4. **Resulting data from experimental tests.**

	Test 2	Test 3	Test 4*
Max system temp at detection (°C)	54.62	54.55	54.15
Max ΔT from induction to detection (°C)	10.45	13.41	-0.67
Time from induction to detection (min)	0.80	0.97	-0.68
Temp increase from max temp required to reach critical temp (°C)	25.38	25.45	25.85

**For the slow-onset blockage in Test 4, blockage induction refers to 95% blockage. Some values are negative due to blockage detection prior to a 95% blockage being reached.*

positives or mask fault signatures.

Furthermore, the time to detection will vary based on the thermal mass, heat capacity, and geometric layout of the monitored system. These factors affect how quickly a blockage manifests as a measurable thermal deviation. Experimental validation in the present work is limited to the representative three-module, parallel-branch architecture shown in Figure 2 and Figure 3. However, the governing formulation in Section III-A is written for $i = 1, \ldots, N$ modules coupled through a coolant network and is driven by measured boundary inputs ($T_{f,\mathrm{in}}, T_\infty, \dot{m}, \{P_i\}$); application to other platforms therefore consists of instantiating the corresponding network topology and calibrating effective thermal parameters and switch thresholds from healthy-operation baselines. Overall, the results confirm that with careful calibration and sufficient model fidelity, the DT can serve as a reliable diagnostic layer for liquid-cooled systems operating in real-world environments. For comparison, a single constant temperature limit would not alarm until the PT had already heated substantially and provides no estimate of the healthy steady-state temperature at the present power and ambient, leading to later or inconsistent detections across operating points.

The simulated transients and the experimental responses are not identical, which is expected given the modeling choices made for embedded execution. The transient branch is a 1-D, well-mixed, lumped thermo-hydraulic network integrated with a backward-Euler scheme at 1 Hz. This introduces spatial averaging and numerical damping, so simulated module and fluid temperatures evolve more slowly than localized sensor readings on the hardware. While a finer nodal discretization configuration could be utilized to reduce negative spatial averaging and numerical damping effects, the increased computational power demand would require the use of more robust, specialized, and expensive hardware, or else would prevent the system from operating in real-time. Additional differences arise from effects that are simplified or omitted in the model, including temperature-dependent properties and convection coefficients, thermal-interface and contact resistances, sensor placement and lag, pump/flow-distribution dynamics, and small ambient variations. Despite these factors, the model captures the dominant trends and the sequence of switch activations; in practice the experiments exhibit earlier detection, while remaining within safe temperature margins. In applications that require faster fault localization or additional discrimination among non-flow-related thermal anomalies, temperature-only DT monitoring can be complemented with pressure/flow or acoustic instrumentation, acknowledging the added hardware and integration cost.

VI. CONCLUSION

This paper presented work on a digital twin-based method of real-time blockage detection in liquid-cooled power electronic systems. Using temperature sensors integrated into the existing hardware, digital twin technology allows for blockage detection without hardware additions. This provides potential facilitation of blockage detection in existing systems with minimal cost, effort, and complexity. Blockage detection was accomplished through the use of five detection switches which detected blockages in simulated tests as early as 10 min post-induction. The system performed at an even

higher capacity in physical testing, detecting blockages in under 1 min for all tests, a 10x increase from simulated tests, and at temperatures roughly 25 °C below the expected failure temperature of 80 °C. This detection was accomplished not only for rapid blockage formation, but also for slow-onset blockages.

Future work will transition the current human-in-the-loop action path to software-mediated closed-loop control and experimentally evaluate automated rectification strategies; such as power redistribution, controlled flow redistribution, or short flow pulses on hardware. These studies will emphasize safety interlocks, thermal-limit compliance, and false-alarm mitigation across operating conditions; the present work validates real-time detection only.

ACKNOWLEDGMENT

This material is based upon work supported by the Office of Naval Research (ONR) under contract numbers N00014-22-C-1003, N00014-23-C-1012, and N00014-24-C-1301. Approved, DCN# 2026-2-23-2011. DISTRIBUTION STATEMENT A. Approved for public release: distribution is unlimited. Any opinions, findings, and conclusions or recommendations expressed in this material are those of the authors and do not necessarily reflect the views of the United States Navy.

REFERENCES

[1] M. Asim *et al.*, "Advancements in thermal management solutions for electric vehicle high-power electronics: Innovations, cooling methods, and future perspectives," *Journal of Energy Storage*, vol. 111, p. 115344, Mar. 1 2025, accessed on April 16, 2025.

[2] M. Akbarzadeh *et al.*, "A comparative study between air cooling and liquid cooling thermal management systems for a high-energy lithium-ion battery module," *Applied Thermal Engineering*, vol. 198, p. 117503, Nov. 5 2021, accessed on April 16, 2025.

[3] A. Castellazzi *et al.*, "Modular assembly of a single-phase inverter based on integrated functional blocks," *IEEE Transactions on Industrial Applications*, vol. 53, no. 6, pp. 5687–5697, Jun. 22 2017, accessed on May 16, 2025.

[4] National Academies of Sciences, Engineering, and Medicine, *Foundational Research Gaps and Future Directions for Digital Twins*. Washington, DC: The National Academies Press, 2024.

[5] E. Glaessgen and D. Stargel, *The Digital Twin Paradigm for Future NASA and U.S. Air Force Vehicles*. [Online]. Available: https://arc.aiaa.org/doi/abs/10.2514/6.2012-1818

[6] J. Voas, P. Mell, P. Laplante, and V. Piroumian, "Security and trust considerations for digital twin technology," National Institute of Standards and Technology, Tech. Rep. NIST IR 8356, 2025.

[7] W. Kritzinger, M. Karner, G. Traar, J. Henjes, and W. Sihn, "Digital twin in manufacturing: A categorical literature review and classification," *IFAC-PapersOnLine*, vol. 51, no. 11, pp. 1016–1022, 2018, 16th IFAC Symposium on Information Control Problems in Manufacturing INCOM 2018. [Online]. Available: https://www.sciencedirect.com/science/article/pii/S2405896318316021

[8] Y. Zeng, Z. A. Hussein, M. H. Chyad, A. Farhadi, J. Yu, and H. Rahbarimagham, "Integrating type-2 fuzzy logic controllers with digital twin and neural networks for advanced hydropower system management," *Scientific Reports*, vol. 15, p. 5140, 2025.

[9] M. Liu *et al.*, "Review of digital twin about concepts, technologies, and industrial applications," *Journal of Manufacturing Systems*, vol. 58, pp. 346–361, Jan. 2021, accessed on April 16, 2025.

[10] F. Tao *et al.*, "Digital twin in industry: state-of-the-art," *IEEE Transactions on Industrial Informatics*, vol. 15, no. 4, pp. 2405–2415, Oct. 1 2018, accessed on May 27, 2025.

[11] G. N. Schroeder, C. Steinmetz, C. E. Pereira, and D. B. Espindola, "Digital twin data modeling with automationml and a communication methodology for data exchange," *IFAC-PapersOnLine*, vol. 49, no. 30, pp. 12–17, 2016, 4th IFAC Symposium on Telematics Applications TA 2016. [Online]. Available: https://www.sciencedirect.com/science/article/pii/S2405896316325538

[12] G. N. Schroeder *et al.*, "A methodology for digital twin modeling and deployment for industry 4.0," *Proceedings of the IEEE*, vol. 109, no. 4, pp. 556–567, Nov. 3 2021, accessed on May 28, 2025.

[13] R. Jedermann *et al.*, "Digital twin concepts for linking live sensor data with real-time models," *Journal of Sensors and Sensor Systems*, vol. 12, no. 1, Apr. 11 2023, accessed on May 29, 2025.

[14] X. Tong *et al.*, "Real-time machining data application and service based on imt digital twin," *Journal of Intelligent Manufacturing*, vol. 31, pp. 1113–1132, Oct. 8 2019, accessed on May 29, 2025.

[15] K. Sado *et al.*, "Query-and-response digital twin framework using a multidomain, multifunction image folio," *IEEE Transactions on Transportation Electrification*, vol. 10, no. 4, pp. 7873–7885, Jul. 8 2024, accessed on April 18, 2025.

[16] F. Tao, B. Xiao, Q. Qi, J. Cheng, and P. Ji, "Digital twin modeling," *Journal of Manufacturing Systems*, vol. 64, pp. 372–389, 2022. [Online]. Available: https://www.sciencedirect.com/science/article/pii/S0278612522001108

[17] M. Attaran and B. G. Celik, "Digital twin: benefits, use cases, challenges, and opportunities," *Decision Analytics Journal*, vol. 6, Mar. 2023, accessed on May 28, 2025.

[18] K. Sado *et al.*, "A digital twin based forecasting framework for power flow management in dc microgrids," *Scientific Reports*, vol. 15, no. 6430, Feb. 21 2025, accessed on May 29, 2025.

[19] K. Sado, J. Peskar, S. Ionita, J. Hannum, A. Downey, and K. Booth, "Real-time electro-thermal simulations for power electronic converters," in *2024 IEEE Applied Power Electronics Conference and Exposition (APEC)*, May 2 2024, pp. 2616–2623, accessed on May 29, 2025.

[20] F. Yang *et al.*, "Digital twin for integration of design-manufacturing-maintenance: an overview," *Chinese Journal of Mechanical Engineering*, vol. 35, no. 80, Jun. 23 2022, accessed on May 28, 2025.

[21] T. Goodwin *et al.*, "Real-time digital twin-based optimization with predictive simulation learning," *Journal of Simulation*, vol. 18, no. 1, pp. 47–64, Mar. 7 2022, accessed on May 29, 2025.

[22] E. J. Tuegel *et al.*, "Reengineering aircraft structural life prediction using a digital twin," *International Journal of Aerospace Engineering*, vol. 2011, no. 1, Oct. 23 2011, accessed on May 29, 2025.

[23] W. Yang *et al.*, "Application status and prospect of digital twin for on-orbit spacecraft," *IEEE Access*, vol. 9, pp. 106 489–106 500, Jul. 27 2021, accessed on May 30, 2025.

[24] E. J. Tuegel, "The airframe digital twin: Some challenges to realization," in *53rd AIAA/ASME/ASCE/AHS/ASC Structures, Structural Dynamics and Materials Conference, 20th AIAA/ASME/AHS Adaptive Structures Conference, 14th AIAA*, Honolulu, HI, USA, Apr. 2012.

[25] J. D. Hochhalter, W. P. Leser, J. A. Newman, and E. H. Glaessgen, "Coupling damage-sensing particles to the digital twin concept," NASA, Tech. Rep. NASA/TM–2014-218257, Apr. 2014, accessed on May 30, 2025. [Online]. Available: https://ntrs.nasa.gov/api/citations/20140006408/downloads/20140006408.pdf

[26] S. Liu *et al.*, "Digital twin modeling method based on biomimicry for machining aerospace components," *Journal of Manufacturing Systems*, vol. 58, no. 2, pp. 180–195, Jan. 2021, accessed on May 30, 2025.

[27] F. Tao, J. Cheng, Q. Qi, M. Zhang, H. Zhang, and F. Sui, "Digital twin-driven product design, manufacturing and service with big data," *International Journal of Advanced Manufacturing Technology*, vol. 94, pp. 3563–3576, 2018, accessed on May 30, 2025.

[28] Y. Lu, C. Liu, I. Kevin, K. Wang, H. Huang, and X. Xu, "Digital twin-driven smart manufacturing: Connotation, reference model, applications and research issues," *Robotics and Computer-Integrated Manufacturing*, vol. 61, p. 101837, 2020, accessed on May 30, 2025.

[29] W. Wen-Hao, C. Guo-bing, and Y. Zi-chun, "The application and challenge of digital twin technology in ship equipment," in *Journal of Physics: Conference Series*, vol. 1939. IOP Publishing, 2021.

[30] Z. Kunkera, T. Opetuk, N. Hadžić, and N. Tošanović, "Using digital twin in a shipbuilding project," *Applied Sciences*, vol. 12, no. 24, p. 12721, 2022.

[31] J. Cronin, E. Santi, A. Wunderlich, and J. Knight, "Fast system level model for digital twin based optimization of naval power and energy system," in *Proceedings of the IEEE Electric Ship Technologies Symposium (ESTS)*, Alexandria, VA, USA, Aug. 2023, pp. 267–273.

[32] J. Worch, K. Sado, A. R. Downey, J. Khan, and E. Santi, "Real-time blockage detection and autonomous recovery in liquid-cooled systems

using digital twins," in *2025 IEEE Electric Ship Technologies Symposium (ESTS)*, 2025, pp. 543–549.

[33] L. Yang *et al.*, "Detection of pipeline blockage using lab experiment and computational fluid dynamic simulation," *Journal of Petroleum Science and Engineering*, vol. 183, p. 106421, Dec. 2019, accessed on Apr. 16, 2025.

[34] X. Zhang *et al.*, "A new strategy for tube leakage and blockage detection using bubble motion-based solid-liquid triboelectric sensor," *Science China Technological Sciences*, vol. 65, pp. 282–292, Nov. 15 2021, accessed on Apr. 16, 2025.

[35] F. Zouari *et al.*, "Internal pipe area reconstruction as a tool for blockage detection," *Journal of Hydraulic Engineering*, vol. 145, no. 6, Mar. 30 2019, accessed on Apr. 18, 2025.

[36] M. Abdullahi and S. O. Oyadiji, "Simulation and detection of blockage in a pipe under mean fluid flow using acoustic wave propagation technique," *Structural Control and Health Monitoring*, vol. 27, no. 4, Jan. 13 2020, accessed on Apr. 18, 2025.

[37] N. Li *et al.*, "Real-time identification and positioning of sewer blockage based on liquid level analysis in rural area," *Environmental and Green Processing*, vol. 11, no. 1, p. 161, Jan. 4 2023, accessed on Apr. 29, 2025.

[38] L. Baronti *et al.*, "Neural network identification of water pipe blockage from smart embedded passive acoustic measurements," *Canadian Journal of Chemical Engineering*, vol. 100, no. 3, pp. 521–539, May 24 2021, accessed on Apr. 29, 2025.

[39] J. Chu *et al.*, "Pressure pulse wave attenuation model coupling waveform distortion and viscous dissipation for blockage detection in pipeline," *Energy Science & Engineering*, vol. 8, no. 1, pp. 260–265, Aug. 12 2019, accessed on May 29, 2025.

[40] A. M. Sattar *et al.*, "Partial blockage detection in pipelines by frequency response method," *Journal of Hydraulic Engineering*, vol. 134, no. 1, Jan. 1 2008, accessed on May 29, 2025.

[41] H.-F. Duan, P. J. Lee, M. S. Ghidaoui, and Y.-K. Tung, "Extended blockage detection in pipelines by using the system frequency response analysis," *Journal of Water Resources Planning and Management*, vol. 138, no. 1, pp. 55–62, 2012.

[42] A. Keramat and R. Zanganeh, "Statistical performance analysis of transient-based extended blockage detection in a water supply pipeline," *Journal of Water Supply: Research and Technology—AQUA*, vol. 68, no. 5, pp. 346–357, 2019.

[43] S. Nasraoui, M. Louati, and M. S. Ghidaoui, "Blockage detection in pressurized water-filled pipe using high-frequency acoustic waves," *Mechanical Systems and Signal Processing*, vol. 185, p. 109817, 2023.

[44] M. Kamal, A. A. Ali, M. Kamel, A. Khalifa, A. Elsisy, H. Ahmed, and M. M. R. Ahmed, "Assessment of the acoustic reflectometry technique to detect pipe blockages," *Journal of Offshore Mechanics and Arctic Engineering*, vol. 143, no. 5, p. 051801, 2021.

[45] H. Yao, D. Li, Y. Li, B. Yang, and Y. Meng, "Blockage detection in pipelines based on linear frequency modulated acoustic reflection method," *Developments in the Built Environment*, vol. 23, p. 100723, 2025. [Online]. Available: https://www.sciencedirect.com/science/article/pii/S2666165925001231

[46] B. Wong and J. A. McCann, "Failure detection methods for pipeline networks: From acoustic sensing to cyber-physical systems," *Sensors*, vol. 21, no. 15, p. 4959, 2021.

[47] R. Hainey, B. Priddy, K. Sado, A. R. J. Downey, J. Khan, H. Fought, and K. Booth, "Digital shadow-based detection of blockage formation in water-cooled power electronics," ser. ASME International Mechanical Engineering Congress and Exposition, vol. Volume 8: Fluids Engineering, 11 2024, p. V008T10A033. [Online]. Available: https://doi.org/10.1115/IMECE2024-142271

[48] "Surface mount stick-on thermocouple, type k, data sheet," The Sensor Connection (Alliance Sensors Group), Tech. Rep., Apr. 2011, rev. 2. [Online]. Available: https://alliancesensors.com/sites/default/files/2021-01/Surface%20Mount%20Stick%20On%20Thermocouple_Type%20K_Data%20Sheet.pdf

JOSIAH WORCH received the B.S. degree in aerospace engineering with honors from the Honors College at the University of South Carolina, Columbia, SC, USA, in 2025. He is currently pursuing the Ph.D. degree in mechanical engineering at the same institution. He is a Graduate Research Assistant in the Department of Mechanical Engineering at the University of South Carolina, working under Dr. Austin Downey. His research focuses on blockage detection for liquid cooling in power electronic systems using digital twins, and more broadly on decision-making frameworks for energy systems. He has published work at the IEEE Electric Ship Technologies Symposium (ESTS).

KERRY SADO received the Ph.D. degree in Electrical Engineering from the University of South Carolina, Columbia, SC, USA, in 2024. He is currently a Research Assistant Professor in the Department of Electrical Engineering at the University of South Carolina, Columbia, SC, USA. He has experience in modeling, simulation, and hardware-in-the-loop applications for power electronics and energy systems. He has contributed to projects involving digital twin technologies, microgrids, and decision-making frameworks for defense-related power and energy systems. Dr. Sado is a Senior Member of the IEEE and has participated in IEEE conferences and contributed to technical program committees in the field of power electronics and energy systems.

AUSTIN DOWNEY received the B.S. degree in Civil Engineering and the Ph.D. degree in Engineering Mechanics; and Wind Energy Science, Engineering, and Policy from Iowa State University. His expertise includes low-latency machine learning, real-time model updating, adaptive structures, and structural health monitoring. His research focuses on online low-latency machine learning through co-design of algorithms and heterogeneous computing hardware for real-time state estimation, time-series forecasting, and anomaly detection. He also investigates real-time decision-making and control for structures in extreme dynamic environments, supported by physics-based models updated in real time, with applications to hypersonic vehicles, active blast mitigation, and orbital infrastructure. Additional work includes smart and adaptive structures that integrate novel sensors and control devices, such as sensing skins, semi-active dampers, and active structural elements, applied to civil infrastructure, transportation systems, and aerospace vehicles. He is also active in in situ monitoring and online validation of additively manufactured components using advanced sensing systems and real-time data assimilation, with applications in fused-filament fabrication (FFF), laser-based additive manufacturing (LBAF), and wire-arc additive manufacturing (WAAM).

JAMIL KHAN received the B.S. degree from the Bangladesh University of Engineering and Technology, the M.S. and Ph.D. degrees from Clemson University, all in Mechanical Engineering. His research interests include modeling of manufacturing processes, temperature distribution during machining, heat transfer and fluid flow with phase change (solidification/melting in casting, welding), computational and experimental fluid dynamics related to contaminants transport in rooms, heat transfer in porous media, micro-channel heat transfer, thermodynamic analysis of IC Engines, CFD analysis of combustion processes etc.

ENRICO SANTI received the B.S. degree from the University of Padua, Italy, the M.S. and Ph.D. degrees from Caltech (California Institute of Technology) in Pasadena, California, all in Electrical Engineering. He has over 25 years of experience in research and development in power electronics, both in industry and in academia. He worked in industry for five years as a Senior Design Engineer, involved in the design of various power supplies for telecommunications and computers, and of electronic ballasts for avionics. He has over 200 publications, three books and four patents. He is currently Transaction Review Chair of the Power Electronics Devices and Components Committee of the IEEE Industry Applications Society. He has been Associate Editor of the IEEE Transactions on Power Electronics and the IEEE Transaction on Industry Applications. His area of research is power electronics. It is a growing research area with many applications from renewable energy to transportation to the power grid. In particular, penetration of power electronics is leading to revolutionary changes in the nature and characteristics of the utility power grid, providing significant research opportunities. His research interests are in control of power electronics power distribution systems, system identification of power electronics systems, physics-based modeling of power semiconductor devices, and modeling and simulation.